

# High energy radiation from luminous and magnetized stars

W. Bednarek

*University of Łódź, Department of Astrophysics, Faculty of Physics and Applied Informatics, ul. Pomorska 149/153, 90-236 Łódź, Poland,  
wlozimirz.bednarek@uni.lodz.pl*

Accepted . Received ; in original form

## ABSTRACT

A part of early type stars is characterised by strong dipole magnetic field that is modified by the outflow of dense wind from the stellar surface. At some distance from the surface (above the Alfvén radius), the wind drives the magnetic field into the reconnection in the equatorial region of the dipole magnetic field. We propose that electrons accelerated in these reconnection regions can be responsible for efficient Comptonization of stellar radiation producing gamma-ray emission. We investigate the propagation of electrons in the equatorial region of the magnetosphere by including their advection with the equatorial wind. The synchrotron and IC spectra are calculated assuming that a significant part of the wind energy is transferred to relativistic electrons. As an example, the parameters of luminous, strongly magnetized star HD 37022 ( $\Theta^1$  Ori C) are considered. The IC gamma-ray emission is predicted to be detected either in the GeV energy range by the Fermi-LAT telescope or in the sub-TeV energies by the Cherenkov Telescope Array. However, since the stellar winds are often time variable and the magnetic axis can be inclined to the rotational axis of the star, the gamma-ray emission is expected to show variability with the rotational period of the star and, on a longer time scale, with the stellar cycle of the magnetic activity. Those features might serve as tests of the proposed scenario for gamma-ray emission from single, luminous stars.

**Key words:** stars: activity — stars: magnetic fields — radiation mechanisms: non-thermal — gamma-rays: stars

## 1 INTRODUCTION

About ten percent of luminous massive stars (OB type) show strong, dipole type magnetic fields (Stahl et al. 1996, Donati et al. 2002), that influence the structure of fast winds from stellar surfaces. A part of the wind, launched in the equatorial region of the star, is focused towards the magnetic equator. Two streams of plasma from opposite hemispheres collide in the equatorial plane heating the medium to temperatures of the order of several  $10^6$  K. (Shore & Brown 1990, Babel & Montmerle 1997, Gagne et al. 2005). On the other hand, the wind launched closer to the polar regions can propagate from the star drawing the magnetic field out. As a result, the winds from massive stars are highly anisotropic as envisaged by e.g. Shore (1987). The polar wind is focused by the magnetic field into the neutral sheet in the equatorial region of the magnetic dipole. It is argued that in this region, electrons are accelerated in the process of magnetic reconnection (e.g. Usov & Melrose 1992). Those electrons are expected to produce non-thermal X-ray radiation. In fact, strong X-ray emission is detected from early type single massive stars (e.g. Pollock 1987, Chlebowski 1989). Relativistic electrons are also expected to produce non-thermal radio emission, observed in the case of 25% of massive stars (e.g. Linsky et al. 1992). The model for the acceleration of electrons in the reconnection regions of the equatorial part of the wind in the outer magneto-sphere of a massive star has been more recently applied to explain its non-thermal radio and X-ray emission (see e.g. Trigilio et al. 2004, Leto et al. 2006, Leto et al. 2017). In this model, electrons are assumed to be accelerated in the reconnection regions in the outer magnetosphere, as postulated by Usov & Melrose (1992). They follow magnetic field lines towards the stellar surface producing synchrotron radiation in the polar regions of the star as observed in the case of Jupiter (Branduardi-Raymont 2007).

Here we apply the general scenario for the acceleration of electrons in the reconnection regions of the outer stellar magnetosphere mentioned above. However, we argue that electrons can reach multi-TeV energies in the reconnection regions. After injection from the reconnection regions, they are isotropised in the random component of the magnetic field present in the equatorial wind. In contrast to Trigilio et al. (2004), we assume that electrons are advected with the equatorial part of the wind in the outward direction from the star. In such general scenario, we consider radiation processes, the synchrotron and the Inverse Compton, which turn to the production of  $\gamma$ -rays. We investigate the conditions for which the high energy radiation, produced in the vicinity of isolated massive star, can be detectable

by the present and future  $\gamma$ -ray observatories. As an example, the case of the nearby, luminous, strongly magnetized star HD 37022 ( $\theta^1$  Ori C) is considered. We show that the parameters of this star allow acceleration of electrons up to TeV energies.

In fact, production of  $\gamma$ -rays in the ICS process of relativistic electrons accelerated in the stellar wind has been already considered from the beginning of the  $\gamma$ -ray astronomy (e.g. White 1985, Pollock 1987). However, another model for the acceleration of electrons in the winds of massive stars has been applied. In the multiple shock in the stellar wind model (originally introduced by Lucy & White 1980 and Lucy 1982), the acceleration of electrons (and hadrons) occurs in the non-stationary wind in which shocks are formed (Chen & White 1991, White & Chen 1992). However, magneto-hydro-dynamic (MHD) simulations of the propagation of the wind do not support formation of such efficient shocks close to the star (e.g. Owocki & Rybicki 1984).

Stars (including the Sun) have been also more recently predicted to be steady sources of  $\gamma$ -rays produced by cosmic ray electrons which IC up-scatter stellar radiation (Moskalenko et al. 2006, Orlando & Strong 2007,2008,2021). In fact, such  $\gamma$ -ray emission has been detected by the EGRET and the Fermi-LAT telescopes (Orlando & Strong 2007, Abdo et al. 2011). The  $\gamma$ -ray emission from the IC process from the nearby super-luminous stars has been also predicted to be within the sensitivity limits of the Fermi-LAT telescope. However, up to now the search of the 12 years of Fermi-LAT data from 9 super-luminous stars in the solar vicinity resulted only in the upper limits which allows to constrain cosmic ray electron spectra in the vicinity of those isolated stars (de Menezes et al. 2021). Luminous stars in dense clusters seems to be stronger emitters of  $\gamma$ -rays, in terms of discussed above scenario, since they are exposed to much stronger density of relativistic electrons accelerated in a turbulent environment (e.g. Ackermann et al. 2011).

## 2 MODEL FOR THE STELLAR WIND/MAGNETIC FIELD INTERACTION

As mentioned above, we apply the general model for the structure of the winds around magnetized luminous stars. It is assumed that the star has ordered (dipole type) structure of the magnetic field. The luminous star produces strong stellar wind which interacts with a strong dipole type magnetic field around the star. We assume that at the considered range of distances from the star, the wind has the velocity which already does not differ significantly

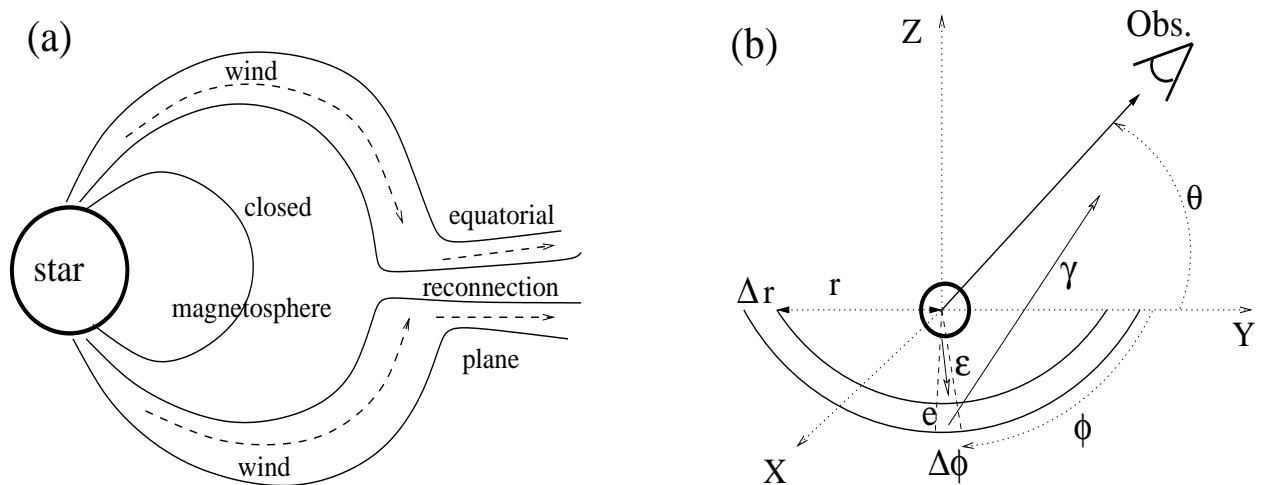


**Figure 1.** Figure (a): Schematic presentation of the considered model. A luminous star produces a dipole magnetic field and launches a strong wind. Close to the star, below the Alfvén radius, the wind flows along the magnetic field lines. Since the energy density of the magnetic field drops faster with the distance from the star than the energy density of the wind, the wind starts to dominate the flow above the Alfvén radius. Then, the magnetic field is forced into reconnection in the equatorial plane. Electrons are accelerated in the reconnection region to maximum energies depending on the velocity of the wind and the magnetic field strength. They are injected with the power law spectrum into the turbulent equatorial region. Electrons lose energy on the synchrotron process (in the random magnetic field) and on the Inverse Compton process (by scattering stellar radiation). Electrons are advected along the equatorial plane with the velocity of the equatorial wind. Figure (b): The geometry of the IC scattering process of stellar radiation ( $\varepsilon$ ) by an electron ( $e$ ) within the narrow ring of the equatorial disk with the radius,  $r$ , the thickness  $\Delta r$ , and at the azimuthal angle  $\phi$  (within the range  $\Delta\phi$ ). Electron ( $e$ ) produces  $\gamma$ -ray photon ( $\gamma$ ) propagating towards the observer located at the angle,  $\theta$ , in respect to the equatorial disk surface.

from the tangent velocity at the infinity. The wind is launched isotropically from the stellar surface with constant density. As a result of the stellar wind/magnetic field interaction, two regions can be defined in the stellar magnetosphere (Babel & Montmerle 1997). Below the so called Alfvén radius, i.e. in the closed magnetosphere, magnetic field drives the wind into the equatorial plane of the magnetic dipole producing two streams of oppositely propagating plasma (see Fig. 1a). The collision of those two streams forms very hot region which emits soft, thermal X-ray emission. This is so called closed magnetosphere. Above the Alfvén radius, the wind drives the magnetic field towards the equatorial region forming the neutral sheet in which reconnection process of the magnetic field can become efficient. We argue that the electric field, induced in the reconnection region, is able to accelerate electrons even to multi-TeV energies.

We consider the example star which is characterised by the mass loss rate as seen at the infinity,  $\dot{M}_w = 4\pi R^2 \rho v_w$ , where the distance from the star is  $R = r R_\star$  with the stellar radius  $R_\star = 10^{12} R_{12}$  cm, the velocity of the wind is  $v_w = 10^8 v_8$  cm s $^{-1}$ , and  $\rho$  is the wind density. The star has dominant dipole magnetic field structure with the strength,  $B(r) = 0.5 B_\star r^{-3}$ , where  $B_\star = 10^3 B_3$  G is the surface magnetic field strength at the magnetic pole. By comparing the energy density of the wind with the energy density of the magnetic field, we estimate

the distance (the Alfvén radius) from the star at which the wind starts to drive frozen in magnetic field. This distance is at,

$$r \approx 3.4(B_3 R_{12})^{1/2} / (\dot{M}_{-6} v_8)^{1/4}, \quad (1)$$

where the mass loss rate of the wind is  $\dot{M}_w = 10^{-6} \dot{M}_{-6} M_\odot \text{ yr}^{-1}$ . Above this distance, the magnetic field, carried by the wind, can efficiently reconnect in the equatorial region of the dipole magnetic field (Usov & Melrose 1992, Trigilio et al. 2004, Leto et al. 2017). At this region, the wind propagates in the outward direction of the star. It can continue flowing in the outward direction forming the equatorial part of the wind as often envisaged in MHD simulations (e.g. ud-Doula & Owocki 2002). Since the stellar winds are expected to be turbulent, electrons injected from the reconnection region are likely isotropised in the wind reference frame.

The maximum energies of electrons accelerated in the reconnection region can be estimated as a product of the induced electric field and the length scale of the reconnection region. The electric field can be parametrised as,  $E_{\text{rec}} = \varepsilon \beta_w c B$ , where  $\beta_w = v_w/c = 0.01 \beta_{0.01}$  is the relative velocity of the wind in respect to the velocity of light  $c$ , and  $\varepsilon = 0.1 \varepsilon_{0.1} \sim 0.1$  is the reconnection efficiency, e.g. Uzdensky (2007). The length scale of the reconnection region can be parametrised by,  $L_{\text{rec}} = \xi R_\star r$  cm, where  $\xi$  is the coefficient describing the extend of the reconnection region defined as a part of distance of the reconnection region from the centre of the star. Then, the maximum energies of electrons are,

$$E_{\text{max}} = E_{\text{rec}} L_{\text{rec}} = 3 \varepsilon_{0.1} \xi \beta_{0.01} B_3 R_{12} r_{10}^{-2} \text{ TeV}, \quad (2)$$

where  $r = 10 r_{10}$  is the distance from the star in units of the stellar radii. We assume that electrons escape with the power law spectrum from the reconnection region into the equatorial wind. The spectrum is characterised by the exponential cut-off,

$$\frac{dN}{dE} = A E^{-\alpha} \exp(-E/E_{\text{max}}), \quad (3)$$

where  $A$  is the normalization constant,  $E_{\text{max}}$  is estimated from Eq. 2, and  $\alpha$  is the spectral index.

In summary, in the considered scenario, electrons are accelerated in the equatorial disk which extends between the range of distances  $R_{\text{min}}$  and  $R_{\text{max}}$  from the star. After isotropisation in the turbulent wind, they are advected in the outward direction from the star. Electrons lose energy on the synchrotron and the IC processes. Electrons, at specific distance,  $R$ , from the centre of the star, comptonize stellar radiation towards the observer

located at the angle  $\theta$  to the disk plane (see Fig. 1b). The effectiveness of the  $\gamma$ -ray production depends on the location of electrons within the disk (defined by the distance,  $R$ , and the azimuthal angle,  $\phi$ ).  $\gamma$ -rays, produced in the IC process, are partially re-absorbed in the stellar radiation.  $\gamma$ -ray spectra are investigated for different parameters of the acceleration model and the location of the observer in respect to the equatorial disk.

### 3 PROPAGATION OF ELECTRONS IN THE EQUATORIAL WIND

Electrons, injected from the reconnection regions, are confined in the plane of the equatorial wind since their Larmor radii, in the local magnetic field, are very small in respect to the typical distance from the star, i.e.

$$R_L = E_{\max}/(eB) \approx 10^{10} \varepsilon_{0.1} \xi \beta_{0.01} R_{12} r_{10} \text{ cm} \ll R, \quad (4)$$

where  $e$  is the charge of the electron. Those electrons are advected with the equatorial wind in the outward direction from the star with the constant wind velocity. Electrons suffer energy losses on the Inverse Compton Scattering of stellar radiation and on the synchrotron process. The relative role of those two energy loss processes (i.e. in the case of IC in the Thomson regime) can be easily estimated by comparing the energy densities of the stellar photons and the magnetic field as a function of distance from the star. The energy density of stellar photons is given by  $\rho_{\text{rad}} \approx 90T_4^4 r^{-2} \text{ erg cm}^{-3}$ , assuming that the stellar radiation is well approximated by the black body spectrum with temperature  $T = 10^4 T_4 \text{ K}$ . The energy density of the magnetic field is  $\rho_B \approx 4 \times 10^4 B_3^2 r^{-6} \text{ erg cm}^{-3}$ . From the comparison of  $\rho_{\text{rad}}$  and  $\rho_B$ , we estimate the distance,

$$r \approx 4.6 B_3^{1/2} / T_4, \quad (5)$$

above which the IC losses (in the Thomson regime) dominate over the synchrotron energy losses. For typical parameters, this distance is larger than the Alfvén radius (Eq. 1). This means that the dominant energy loss process of electrons is synchrotron radiation in the inner part of the equatorial wind. The IC process (in the Thomson regime) dominates at farther distances from the star. Note however, that in the Klein-Nishina regime, i.e. for electrons with energies above  $E_e \sim 100/T_4 \text{ GeV}$ , the synchrotron process becomes important even at large distances from the star.

We also estimate of the optical depth on the Inverse Compton scattering of stellar radiation by relativistic electrons in order to have impression how efficiently energy is transferred

from relativistic electrons to the high energy radiation. The optical depth can be estimated from,  $\tau = n_{\text{ph}}\sigma_{\text{T}}R \approx 1.3T_4^3R_{12}r_{10}^{-1}$ , where  $n_{\text{ph}} \approx 1.9 \times 10^{11}T_4^3r_{10}^{-2} \text{ cm}^{-3}$  is the density of stellar photons. We conclude that a significant amount of electron's initial energy is transferred to the high energy  $\gamma$ -rays in the IC process, provided that the surface temperature of the luminous star is clearly above  $10^4$  K.

In order to follow the advection process of electrons, we divide the equatorial disk on a sequence of rings with the radius  $r$  and the thickness  $0.2r_*$ . Electrons are assumed to be injected at a specific element of the ring defined by the azimuthal angle  $\phi$  (measured from the location of the observer, see Fig. 1b).

#### 4 RADIATION FROM ELECTRONS

In order to calculate the  $\gamma$ -ray spectra, produced by electrons in the comptonization of stellar radiation, we modify the numerical Monte Carlo code for the development of the IC  $e^\pm$  pair cascade initiated by relativistic electrons in the anisotropic radiation from the luminous star, originally developed by Bednarek (1997,2006). The code calculates the  $\gamma$ -ray spectra from electrons located at a specific distance from the stellar surface.  $\gamma$ -rays escape towards the observer located at an arbitrary angle to the direction between the electron and the centre of the star. It takes into account the Inverse Compton process and the  $e^\pm$  pair production by  $\gamma$ -rays in collision with stellar radiation. In the present calculations, we limit the IC  $e^\pm$  pair cascade process to the first generation of produced  $\gamma$ -rays in the IC process since it becomes very complicated to follow emission from secondary  $e^\pm$  pairs in complex structure of the magnetic field influenced by the out-flowing stellar wind in the present scenario. The structure of the magnetic field can strongly influence the paths of secondary cascade  $e^\pm$  pairs, re-distributing directions of secondary  $\gamma$ -rays (e.g. Sierpowska & Bednarek 2005). Therefore, the  $\gamma$ -ray spectra, obtained in our scenario, should be considered as lower limits, especially at their low energy part. Due to the anisotropic radiation field of the star (as seen from the location of relativistic electrons), the  $\gamma$ -ray spectra from the IC process depend on the inclination angle of the observer in respect to the equatorial disk.

The synchrotron spectra are obtained assuming dominant random magnetic field in the equatorial disk outside smaller scale coherent reconnection regions. The cooling process of electrons, injected with energy  $E_e(r)$ , is followed up to the moment of their advection from the disk or their cooling to the energy  $E_{\text{min}} = 1$  GeV. Electrons with  $E_{\text{min}}$  are not able

to produce  $\gamma$ -rays above 100 MeV in the IC process. Due to a relatively small velocity of the equatorial wind (beaming of radiation not essential) and the assumption on the random magnetic field within the disk, the synchrotron emission is isotropic.

As we mentioned above, relativistic electrons are injected within the thin disk laying in the equatorial plane of the dipole magnetic field. Electrons have a power law spectrum defined by the spectral index, the maximum energy determined by the conditions within the disk, and the power corresponding to ten percent of the power of the stellar wind (Usov & Melrose 1992). This normalization to the wind power bases on the assumption that the wind is launched isotropically from the stellar surface. We estimate a part of this isotropic wind which falls onto the  $n$ 'th ring extending between distances  $R_n$  and  $R_{(n+1)}$  (see also Trigilio et al. 2004). The thickness of the ring has been chosen on  $\Delta R = 0.2r_*$ , i.e.  $R_{(n+1)} = R_n + 0.2R_*$ . The equation of a specific magnetic field line, with the dipole structure, is given by  $R_* = R_n \sin^2 \lambda_n$ , where  $\lambda_n$  is the angle between the magnetic pole and the starting point of the magnetic field line extending to  $R_n$ , and  $R_n$  is the distance measured in the equatorial plane of the magnetic dipole. We want to derive a part of the solid angle between the magnetic field lines starting at the angles  $\lambda_n$  and  $\lambda_{(n+1)}$ . They correspond to the extend of the ring. This part of the whole solid angle is  $\Delta\Omega/(4\pi) = 0.5(\cos \lambda_n - \cos \lambda_{(n+1)})$ . Only this part of the wind, launched from the star, falls onto the ring within the radii  $R_n$  and  $R_{(n+1)}$ .

Electrons are quickly isotropised by a turbulent magnetic field within the equatorial disk. They are assumed to lose energy on two processes. The synchrotron process in the local magnetic field and the IC process in the anisotropic radiation field of the stellar radiation. We assume that electrons lose energy continuously on the synchrotron process up to the moment of the first production of  $\gamma$ -ray photon. The energy and emission angle of produced  $\gamma$ -ray photon is counted in order to produce angular dependent  $\gamma$ -ray spectra in respect to the equatorial disk. In this calculations, we also take into account the change of the position of the electron on the equatorial disk surface due to their advection process outside the equatorial wind. The cooling process of electrons and the process of  $\gamma$ -ray production is followed by applying the Monte Carlo method. We calculate the  $\gamma$ -ray spectra from every element of the ring. The location of this surface element is defined by the distance from the star,  $R$ , and the azimuthal angle,  $\phi$ , in respect to the location of the observer, whose position is defined by the inclination angle,  $\theta$ , to the plane of the equatorial disk.



## 5 APPLICATION TO HD 37022 ( $\theta^1$ ORI C)

We apply the model for the example luminous, magnetized O type star. We select the parameters of the star in the way that the acceleration of electrons in the reconnection region is possible to TeV energies (see Eq. 2). Moreover, the radiation field of this example star has to guarantee efficient IC scattering of stellar radiation by those electrons (i.e. optical depth above unity, see Sect. 3). As noted in the introduction, significant part of massive stars show strong magnetic field. Detailed structure and strength of the field is precisely measured only in the case of several O type stars (see Table 1 in Chandra et al. 2015 and Petit et al. 2013). The best parameters, from the modelling point of view, has the star HD 37022, which is also known as  $\Theta^1$  Ori C. From another side,  $\Theta^1$  Ori C is a problematic target for  $\gamma$ -ray telescopes since it is the most luminous star in the Trapezium cluster which is a part of the Orion Molecular Complex. The Orion Complex is well established very extended  $\gamma$ -ray source (Ackermann et al. 2012a,2012b). Therefore, investigation of a point like  $\gamma$ -ray source in front of the extended  $\gamma$ -ray source can become problematic for the analysers of the Fermi-LAT data. The basic parameters of the main star in  $\Theta^1$  Ori C, such as the radius  $R_\star$ , the surface temperature  $T_\star$  (Simón-Díaz et al. 2006), the dipole magnetic field strength at the pole  $B_\star$  (Wade et al. 2006), the wind velocity  $v_w$ , and the mass loss rate  $\dot{M}_w$  (Petit et al. 2013), are given in Tab. 1. For the above parameters, the wind power is  $L_w = \dot{M}_w v_w^2 / 2 \approx 1.56 \times 10^{36}$  erg s $^{-1}$ . The distance to HD 37022 is equal to 410 pc (Kraus et al. 2009). In fact, HD 37022 is a binary system in which less luminous B type star has a relatively low mass loss rate. Separation of the companion stars at the periastron passage is  $(1 - e)a \approx 2.8 \times 10^{14}$  cm, for the semi-major axis of the binary system  $a = 40$  AU and the eccentricity  $e = 0.534$  (Kraus et al. 2009). This is clearly larger than the distance scale of the colliding wind around HD 37022. Therefore, we conclude that the presence of the companion star in this binary system does not influence processes in the inner magnetosphere around more luminous companion HD 37022.

For the above parameters, the closed magnetosphere around HD 37022 extends only to  $2.4R_\star$ . Above this distance, the magnetized wind of HD 37022 forms good conditions for efficient reconnection of the stellar magnetic field. In these reconnection regions, electrons are expected to be accelerated to multi-TeV energies. After initial acceleration process in the reconnection regions, electrons are slowly advected along the equatorial wind region in the outward direction from the star. They lose energy on the synchrotron radiation and the

**Table 1.** Parameters of the star HD 37022 ( $\theta^1$  Ori C)

$R_*$ (cm)	$T_*$ (K)	$B_*$ (G)	$\dot{M}$ ( $M_\odot/\text{yr}$ )	$v_w$ (cm/s)
$7 \times 10^{11}$	$3.9 \times 10^4$	$1.1 \times 10^3$	$5 \times 10^{-7}$	$3.225 \times 10^8$

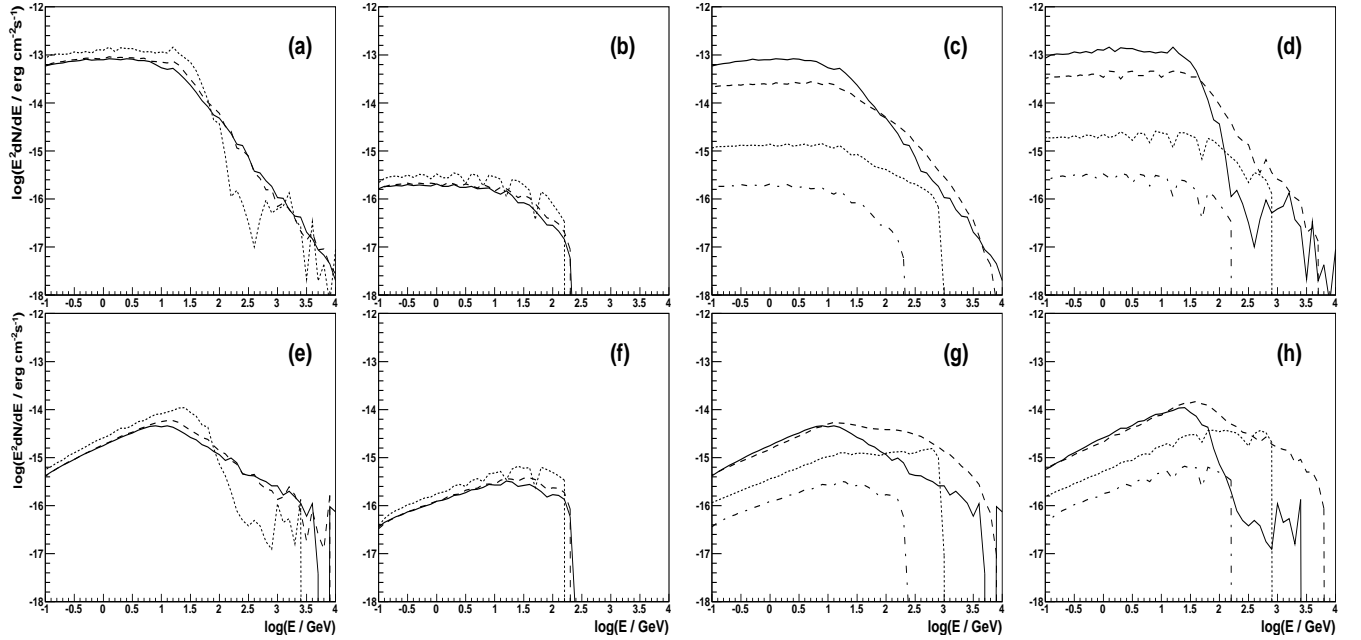


**Figure 2.** Gamma-ray spectra produced by relativistic electrons in the IC scattering process of thermal radiation from the star with the example parameters of HD 37022 (see Table 1). Electrons are accelerated in the reconnection region extending in the plane perpendicular to the axis of the dipole magnetic field of the star. Electrons are injected from the reconnection regions in the equatorial wind region with the power spectrum characterised by the spectral index,  $\alpha$ , up to the maximum energy,  $E_{\max}$ , defined by Eq. 2. Electrons are injected at specific distances from the surface of the star: (panel a)  $R = 2.5R_*$  and  $\alpha = 2$ ; (e)  $R = 2.5R_*$  and  $\alpha = 1$ ; (b)  $R = 30R_*$  and  $\alpha = 2$ ; (f)  $R = 30R_*$  and  $\alpha = 1$ ; for three inclination angles of the direction towards the observer in respect to the disk plane:  $\theta = 15^\circ$  (solid curves),  $45^\circ$  (dashed), and  $90^\circ$  (dotted). The dependence of the  $\gamma$ -ray spectra on the distance from the star,  $R = 2.5R_*$  (solid),  $5R_*$  (dashed),  $15R_*$  (dotted) and  $30R_*$  (dot-dashed), for two selected inclination angles of the observer,  $\theta = 15^\circ$  and  $90^\circ$ , is shown in panels (c) and (d) for  $\alpha = 2$  and (g) and (h) for  $\alpha = 1$ , respectively. The synchrotron energy losses of electrons, during their advection process along the equatorial wind region, are taken into account. The magnetic field strength in the equatorial wind is derived assuming its global dipole structure described by  $B = 0.5 \times B_*(R_*/R)^3$ . The spectrum of electrons is normalized to 10% of the part of the wind power,  $L_w = 1.56 \times 10^{36}$  erg s $^{-1}$ , which arrive to the equatorial plane at the ring with the inner radius  $R$  and thickness  $0.2R_*$ .

inverse Compton up-scattering of thermal radiation from the nearby surface of the luminous star.

At first, we calculate the  $\gamma$ -ray spectra produced by electrons which are injected at the ring defined by the specific range of distances from the star. According to the considered scenario, electrons are accelerated in the reconnection regions to larger energies closer to the star due to the strong dependence of the dipole magnetic field on the distance from the star. However,  $\gamma$ -rays, produced by them in the IC process closer to the star, are also more efficiently absorbed in the stellar radiation. Therefore, the  $\gamma$ -ray spectra show complicated behaviour with the distance from the star. On Figs. 2a,b and 2e,f, we investigate dependence of the IC  $\gamma$ -ray spectra on the location of the external observer in respect to the plane of

**Table 2.** Parameters of the models for electron acceleration

model:	$\alpha$	$\xi$	$E_{\max}(R_{\text{in}} = 2.4R_{\star})$	$E_{\max}(R_{\text{out}} = 30R_{\star})$
I	2	1	40 TeV	260 GeV
II	1	1	40 TeV	260 GeV
III	1	0.1	4 TeV	26 GeV

the equatorial wind for two models of the spectrum of electrons, described by the spectral index equal to  $\alpha = 2$  (2a,b) and  $\alpha = 1$  (2e,f). The  $\gamma$ -ray spectra, produced closer to the star (the case for  $R = 2.5R_{\star}$ ), show strong dependence on the inclination angle due to strongly dependent conditions for their absorption in the stellar radiation. Only a part of the TeV  $\gamma$ -rays is able to escape from the stellar radiation field. The most favourite conditions for the escape of  $\gamma$ -ray photons are from the part of the equatorial disk which lays in front of the star in respect to the external observer (the interaction angle between the  $\gamma$ -ray photon and the stellar photon is the largest). On the other hand,  $\gamma$ -ray spectra, produced at large distances from the star, extend only to sub-TeV energies. Their level is within a factor of two for the range of angles between  $\theta = 15^{\circ} - 90^{\circ}$  (see Fig. 2bf for  $R = 30R_{\star}$ ). The weakest spectra are observed for small inclination angles of the observer. In fact, weak dependence of the  $\gamma$ -ray spectra on the observation angle,  $\theta$ , is not so surprising. They are produced in specific parts of the ring as a result of the IC scattering of stellar radiation arriving at quite large range of angles. Therefore,  $\gamma$ -ray emission from the whole ring is averaged over large range of collision angles. In Figs. 2, we also show the dependence of the  $\gamma$ -ray spectra on the distance from the star for two fixed inclination angles,  $\theta = 15^{\circ}$  (Figs 2c,g) and  $90^{\circ}$  (Figs. 2d,h). We show that  $\gamma$ -ray spectra are produced with the largest energies, extending to the TeV range, at the intermediate distances from the star (for example see the case for  $R \sim 5R_{\star}$ ). Instead, electrons are accelerated to the largest energies at the inner radius of the equatorial disk. This effect is due to efficient absorption of  $\gamma$ -rays in the stellar radiation, with energies close to  $\sim 100$  GeV. Also, the dominant synchrotron energy losses of electrons (in comparison to the IC losses) in the inner part of the equatorial disk plays an essential role in drawing energy from electrons at the inner radius of the equatorial disk.

In the next step, we calculate the  $\gamma$ -ray spectra produced by electrons in the IC process from the whole equatorial wind region. As an example, we select the disk with the inner radius corresponding to the Alfvén radius in the magnetosphere of the star HD 37022 (i.e.  $2.4R_{\star}$ ) and the outer radius fixed on  $30r_{\star}$ . The outer radius is chosen in order to be

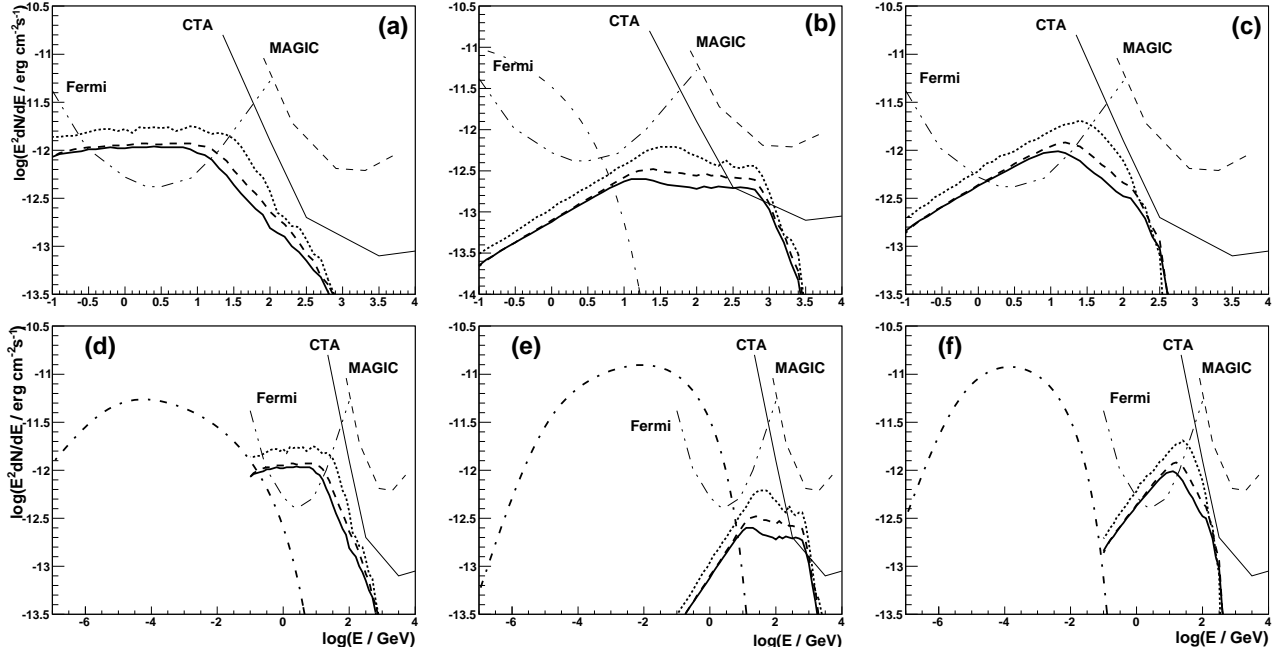


**Figure 3.** Gamma-ray spectra produced by relativistic electrons in the equatorial wind region between the range of distances from the star  $R_{\min} = 2.5R_{\star}$  and  $R_{\max} = 30R_{\star}$ . Electrons IC up-scatter thermal radiation from the star with the parameters of HD 37022. Electrons are injected, from the reconnection regions in the equatorial wind, with the power law spectrum defined by the spectral index  $\alpha$  and maximum energies  $E_{\max}$ . The synchrotron energy losses of electrons, during their advection process along the equatorial wind, are included. Three models for the electron acceleration and considered. Model I: the spectral index is  $\alpha = 2$  and the length of the reconnection region is  $\xi = 1$ , see figure (a) for the synchrotron and the IC spectra and (d) for details of IC spectra. Model II:  $\alpha = 1$  and  $\xi = 1$  (figures (b) and (e), respectively). Model III:  $\alpha = 1$  and  $\xi = 0.1$  (figures (b) and (e) respectively). Specific lines show the results for three inclination angles of the distant observer in respect to the plane of the equatorial disk:  $\theta = 15^\circ$  (solid curve),  $45^\circ$  (dashed), and  $90^\circ$  (dotted). It is assumed that the magnetic field at the equatorial wind region is defined by the dipole structure. The spectrum of electrons is normalized to 10% of the wind power,  $L_w = 1.56 \times 10^{36} \text{ erg s}^{-1}$ , which arrive to the equatorial plane between  $R_{\min}$  and  $R_{\max}$ . The gamma-ray spectra are confronted with the sensitivities of the Fermi-LAT (10 yrs, see dot-dot-dashed curve, Funk et al. 2013), the MAGIC array (50 hrs, thin dashed curve, Aleksić et al. 2012) and the planned CTA array (50hrs, thin solid curve, Maier et al. 2017).

consistent with the distance at which the structure of the magnetic field around the star changes to toroidal. At this distance, acceleration of electrons in the reconnection regions in the equatorial disk can still occur to energies of the order of  $\sim 100 \text{ GeV}$  (i.e. produced by them  $\gamma$ -rays can reach energies within sensitivities of the Cherenkov telescopes). We consider three models for the acceleration of electrons and for their subsequent energy losses during advection with the equatorial wind. In all models, electrons are injected from the reconnection regions with the power law spectrum with the exponential cut-off at energy  $E_{\max}$ . This maximum energy depends on the local magnetic field strength at the equatorial disk (i.e. depends on  $R$ ) and on the length scale,  $\xi$ , of the reconnection region. Spectra of relativistic electrons are normalized to 10% of the wind power which propagates towards the equatorial disk. The parameters of specific models are reported in Tab. 2.

We perform calculations of the  $\gamma$ -ray and synchrotron spectra, in terms of the considered model for those three sets of example parameters. The spectra are shown in Fig. 3 for three

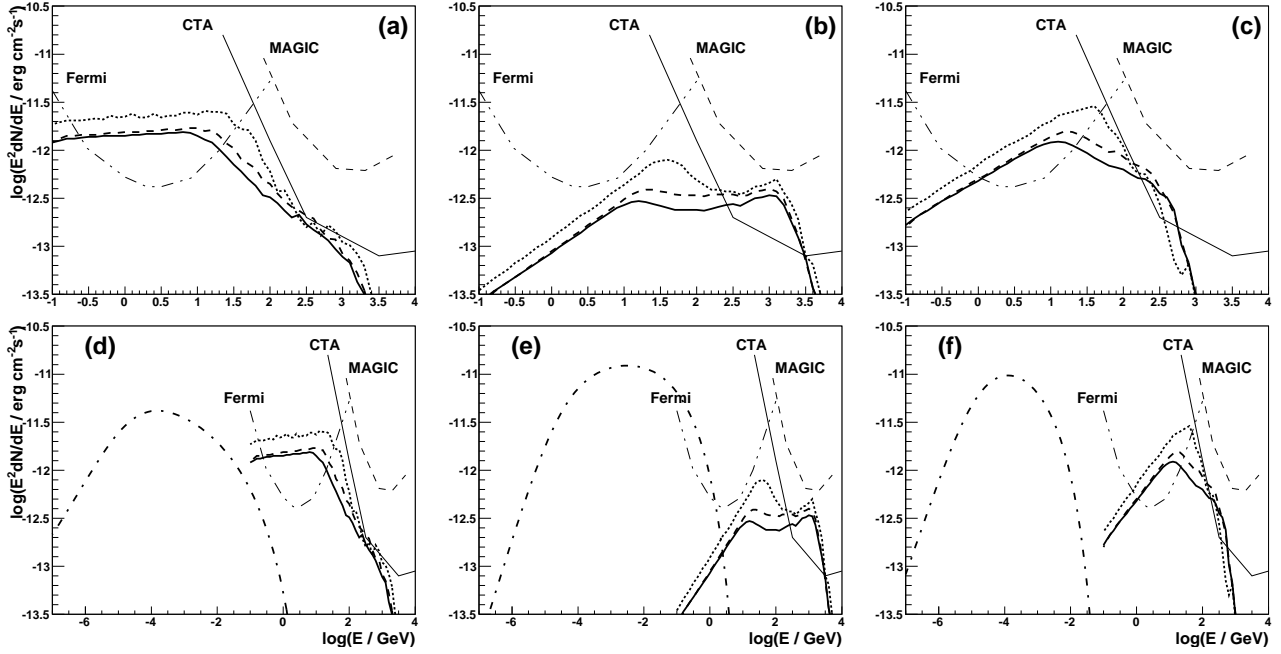


Figure 4. As in Fig. 3 but for the reduction factor of the magnetic field strength in the equatorial wind equal to  $\mu = 0.3$ .

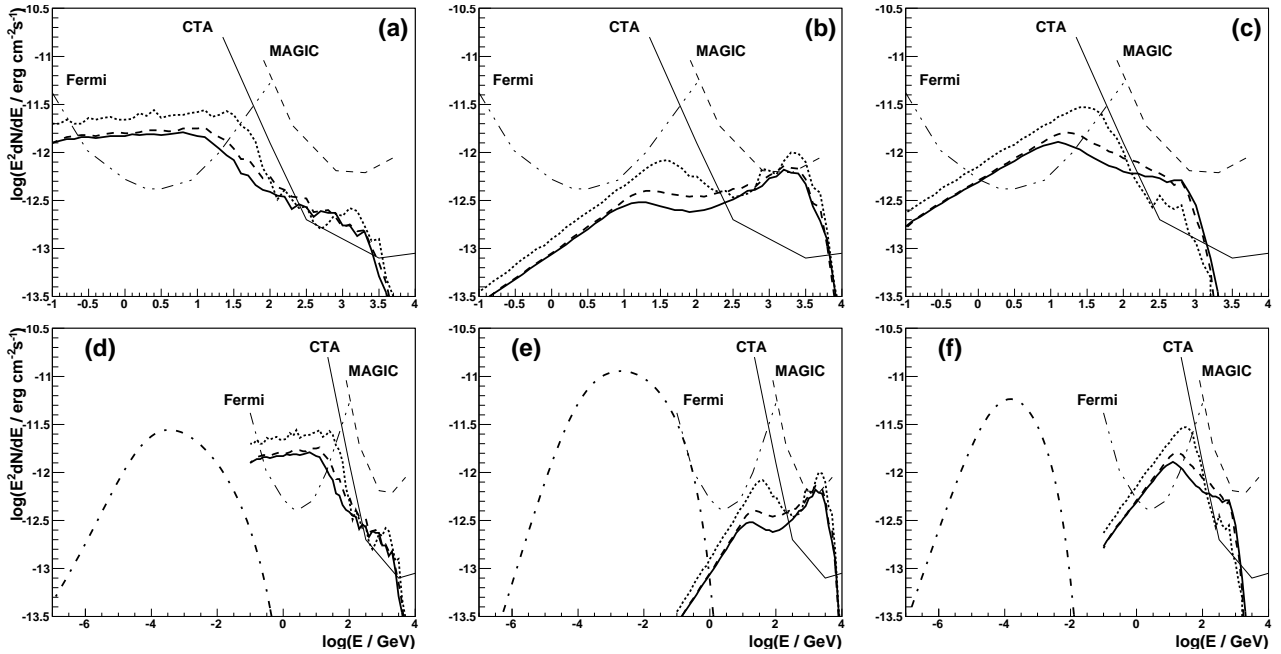


Figure 5. As in Fig. 3 but for the reduction factor of the magnetic field strength in the equatorial wind region equal to  $\mu = 0.1$ .

inclination angles of the distant observer in respect to the plane of the equatorial disk:  $\theta = 15^\circ$  (solid curve),  $45^\circ$  (dashed), and  $90^\circ$  (dotted). The results are confronted with the sensitivities of the present (Fermi-LAT , MAGIC) and future (CTA)  $\gamma$ -ray telescopes. In the case of the model I (Fig. 3ad), the  $\gamma$ -ray spectra extend through the GeV energy range with the fast decline above  $\sim 30$  GeV. Such emission can be detected by the Fermi-LAT

telescope. However, the sub-TeV emission is clearly below the sensitivity of the future CTA. On the other hand, in the model II (Fig. 3be), the GeV  $\gamma$ -ray emission is predicted to be below sensitivity of the Fermi-LAT, but it might be marginally detected at energies close to  $\sim 1$  TeV by the CTA. The injection of electrons with the hard spectrum, but lower acceleration efficiency (model III, Fig. 3cf), turns to the  $\gamma$ -ray emission which is expected to have features similar to those presented in model I. However, the GeV spectrum is flatter, steepening more suddenly in the sub-TeV range.

The synchrotron emission is expected to dominate over the IC  $\gamma$ -ray emission in all considered models. Interestingly, in the model II, the tail of the synchrotron emission extends up to GeV energies. This part of the synchrotron spectrum dominates completely over a part of the spectrum produced in the IC process.

In fact, strong thermal X-ray emission is observed from HD 37022 (Gagne et al. 2005). It has been predicted to originate in the inner (closed) part of the magnetosphere, in which the winds, launched from the regions of magnetic poles, should collide in the equatorial region. As a result of this collision, strong, soft X-ray emission is produced. This soft X-ray emission dominates the energy output of the star. Predicted by our model broad band non-thermal synchrotron component, extending from the soft X-rays up to  $\gamma$ -rays, is dominated by the thermal soft X-ray emission from the inner magnetosphere.

In fact, magnetic field in the equatorial wind can be significantly reduced from the values delivered by the stellar dipole magnetic field to the reconnection regions, since a part of the magnetic energy has to be transferred to relativistic particles and thermal plasma. Therefore, we also consider the cases in which electrons, injected from the reconnection regions into the equatorial wind, produce synchrotron and IC radiation in the region of significantly reduced magnetic field (by a factor of  $\mu$ ). We investigate the synchrotron and the IC spectral features assuming that the reduction factor is equal to  $\mu = 0.3$  (Fig. 4) and  $\mu = 0.1$  (Fig. 5), for all three models of the electron injection, as considered in the case without magnetic field reduction (Fig. 3 calculated for  $\mu = 1$ ). If the effect of the magnetic field reduction is important, then the synchrotron emission is predicted to be on a much lower level. On the other hand, the IC  $\gamma$ -ray emission appears stronger. For  $\mu = 0.1$ , the tail of synchrotron emission is not expected to be detected by the Fermi-LAT telescope even in terms of the model II. On the other hand, sub-TeV  $\gamma$ -ray emission reaches the level allowing its detection by the CTA in the case of all considered models. In the case of the model II, the peak of

the IC  $\gamma$ -ray emission is even within the sensitivity of the present MAGIC telescope around TeV energies.

## 6 DISCUSSION AND CONCLUSION

We investigate the high energy radiation processes of relativistic electrons injected from the reconnection regions in the colliding winds around massive, magnetized star applying, as an example, the parameters of the star HD 37022 (known also as  $\theta^1$  Ori C). Following previous investigations (e.g. Usov & Melrose 1992, Trigilio et al. 2004), we assume that reconnection regions appear in the equatorial wind formed as a result of collisions of winds launched from the two magnetic poles of the star. Relativistic electrons are captured in the turbulent equatorial wind. They are advected with the wind in the outward direction from the star, suffering energy losses on the synchrotron process and on the IC scattering of stellar radiation. We calculate the synchrotron and the IC  $\gamma$ -ray spectra produced by these electrons in the case of a few models for the electron acceleration and propagation in the wind. We show that for the specific conditions, this  $\gamma$ -ray emission can be detected either in the GeV energy range by the Fermi-LAT telescope or by the future Cherenkov Telescope Array at sub-TeV energies, provided that close to 10% of the wind power is transferred to relativistic electrons. If the acceleration process of electrons in the reconnection regions is very efficient (flat spectrum with spectral index close to  $\alpha = 1$  and maximum energy at TeV energy range), then very steep high energy tail of the synchrotron emission might be even detected at GeV energies by the Fermi-LAT.

$\gamma$ -ray emission has been discovered in the GeV (and also TeV) energies from the direction of a few types of stellar objects (see e.g. Abdollahi et al. 2020). Two massive binary systems, Eta Carinae (e.g. Tavani et al. 2009, Abdo et al. 2010) and  $\gamma^2$  Velorum (Pshirkov 2016) have been discovered in the GeV energy range. Eta Carinae has been also observed recently in the TeV energies (Abdalla et al. 2020). Moreover, Fermi-LAT and Agile telescopes detected GeV emission from a few binary systems containing compact objects. Some of them have been already discovered in the TeV energies. Between them, the best investigated are LSI 61+303 (Albert et al. 2006, Abdo et al. 2009a) and LS5039 (Aharonian et al. 2005a, Abdo et al. 2009b). In the case of another binary system, PSR1259-63/SS2883 (e.g. Tam et al. 2011, Aharonian et al. 2005b), the compact object is well documented as a rotation powered neutron star. To my knowledge any single, isolated star is observed in  $\gamma$ -rays up to now.

However, in the case of binary systems, proposed here model for the high energy  $\gamma$ -ray emission can provide additional component to the high energy emission expected from a large scale shock formed as a result of collisions of stellar winds within the binary system (see e.g. Eichler & Usov 1993, Benaglia & Romero 2003, Bednarek 2005, Reimer et al. 2006, Pittard & Dougherty 2006, Farnier et al. 2010, Bednarek & Pabich 2011). In fact, both processes of electron acceleration (i.e. shock acceleration on the large scale double shock structure within the binary and the reconnection in the wind of the magnetized star) can contribute to the emission from specific stellar binary systems and also binary systems of massive stars with compact objects (neutron stars, black holes). As argued in the above mentioned works, also hadrons can contribute to the  $\gamma$ -rays in the interaction with the matter of dense winds or in stellar atmospheres. Therefore, it is not surprising that the high energy emission from massive binary systems can show very complicated features. In fact, a few emission components are expected to appear in different phases of the binary system, since all those processes depend significantly on their parameters and viewing geometry.

In our calculations, we assumed steady conditions in the equatorial wind. However, the stellar winds are often non-stationary and time dependent. Moreover, the dipole magnetic field can vary on a longer time scale. In such a case, the conditions in the wind around the specific star can change drastically. This should have serious effect on the stability of predicted here features of the  $\gamma$ -ray emission. For more powerful winds, the inner radius of the equatorial disk is expected to shift towards the star. More power is expected to be transferred to relativistic electrons. However, electrons will lose energy more efficiently on the synchrotron process in stronger magnetic field. So then, produced IC  $\gamma$ -ray spectra are expected on a higher level but they are limited to lower energies, without significant sub-TeV component. If the dipole magnetic field of the star becomes weaker from some reasons, then the inner radius of the equatorial disk should also move closer to the star. In such a case, synchrotron energy losses of electrons are expected on a similar level but more energy is transferred from the wind to electrons. Then, the  $\gamma$ -ray spectrum is expected to strengthen and shifts to higher energies. This should allow easier detection of the sub-TeV  $\gamma$ -ray emission by the Cherenkov telescopes.

Another complication is due to the inclination of the magnetic dipole axis to the rotational axis of the star. In such a case, the viewing angle of the equatorial disk by a distant observer changes regularly with the rotation period of the star (which is equal in the case of HD 37022 to 15.4 days, Stahl et al. 1993). In the case of HD 37022, the magnetic dipole



axis is inclined at the angle  $42^\circ$  and the observer is located at the angle  $45^\circ$  in respect to the rotational axis of the star (Gagne et al. 2005). Therefore, the viewing angle of the equatorial disk by the observer changes from  $3^\circ$  (nearly pole on) up to  $87^\circ$  (nearly equatorial disk on) during the rotational period of the star. For such parameters, we predict the periodic fluctuation of the level of  $\gamma$ -ray emission (mainly at a few tens of GeV) with the rotational period of the star by a factor close to  $2 - 3$  (see spectra on Figs. 3-5).

In the specific case of the example star,  $\theta^1$  Ori C, the  $\gamma$ -ray emission discussed here is expected below the extended GeV  $\gamma$ -ray emission, recently observed from the Orion Molecular Complex by the Fermi-LAT and Agile satellites (Ackermann et al. 2012a,2012b, Marchili et al. 2018). However, chances of detection of the TeV  $\gamma$ -ray emission by the Cherenkov telescopes, over the presumed extended background emission from the Orion Molecular Complex, are expected to be better due to superior angular resolution of the Cherenkov telescopes. In fact, recently predicted extended TeV  $\gamma$ -ray flux from the Orion Molecular Complex (Aharonian et al. 2020) is on the level of the TeV  $\gamma$ -ray flux expected in our calculations for HD 37022 ( $\theta^1$  Ori C). Recent upper limit on the TeV  $\gamma$ -ray emission from the Orion Molecular Complex, reported by the HAWC Observatory (Albert et al. 2021), is clearly above those predictions.

## ACKNOWLEDGMENTS

I would like to thank the Referee for many useful comments. This work is supported by the grant through the Polish National Research Centre No. 2019/33/B/ST9/01904.

## DATA AVAILABILITY

The simulated data underlying this article will be shared on reasonable request to the corresponding author.

## REFERENCES

- Abdalla, H., Adam, R., Aharonian, F. et al. 2020 A&A 635, 167  
 Abdo, A.A., Ackermann, M., Ajello, M. et al. 2009a ApJ 701, 123L  
 Abdo, A.A., Ackermann, M., Ajello, M. et al. 2009b ApJ 706, L56  
 Abdo, A.A., Ackermann, M., Ajello, M. et al. 2010 ApJ 723, 649  
 Abdo, A.A., Ackermann, M., Ajello, M. et al. 2011 ApJ 734, 116  
 Abdollahi, S., Acero, F., Ackermann, M. et al. 2020 ApJS 247, 33

- Ackermann, M., Ajello, M., Allafort, A., et al. 2011 *Science* 334, 1103
- Ackermann, M., Ajello, M., Allafort, A., et al. 2012a *ApJ*, 756, 4
- Ackermann, M., Ajello, M., Allafort, A., et al. 2012b *ApJ*, 755, 22
- Aharonian, F., Akhperjanian, A. G., Aye, K. -M. et al. 2005a *Science* 309 746
- Aharonian, F., Akhperjanian, A. G., Aye, K. -M. et al. 2005b *A&A* 442 1
- Aharonian, F., Peron, G., Yang, R., Casanova, S., Zanin, R. 2020 *PRD* 101, 083018
- Albert, A., Aliu, E., Anderhub, H. et al. 2006 *Science* 312 1771
- Albert, A., Alfaro, R.; Alvarez, C. et al. 2021 *ApJ* 914, 106
- Aleksić, J., Alvarez, E. A.; Antonelli, L. A. et al. 2012, *APh* 35, 435
- Babel, J., Montmerle, T. 1997 *ApJ* 485, L29
- Bednarek, W. 1997 *A&A* 322, 523
- Bednarek, W. 2005 *MNRAS* 363, 46
- Bednarek, W. 2006 *MNRAS* 368, 579
- Bednarek, W., Pabich, J. 2011 *A&A* 530, 49
- Benaglia, P. & Romero, G.E. 2003 *A&A* 399, 1121
- Branduardi-Raymont, G., Bhardwaj, A., Elsner, R.F., Gladstone, G.R., Ramsay, G., Rodriguez, P., Soria, R., Waite, J.H., Jr., Cravens, T.E. 2007 *A&A* 463, 761
- Chandra, P., Wade, G.A., Sundqvist, J.O. et al. 2015 *MNRAS* 452, 1245
- Chen, W., White, R.L. 1991 *ApJ* 381, 63
- Chlebowski, T. 1989 *ApJ* 342, 1091
- de Menezes, R., Orlando, E., Di Mauro, M., Strong, A. 2021 in press, DOI:10.1093/mnras/stab2150
- Donati, J.-F., Babel, J., Harries, T.J., Howarth, I.D., Petit, P., Semel, M. 2002 *MNRAS* 333, 55
- Eichler, D., & Usov, V. 1993 *ApJ*, 402, 271
- Farnier, C., Walter, R., Leyder, J.-C. 2010 *A&A* 526, A57
- Funk, S., Hinton, J.A. (CTA Consortium) 2013, *APh* 43, 348
- Gagné, M., Oksala, M.E., Cohen, D.H., Tonnesen, S.K., ud-Doula, A., Owocki, S.P., Townsend, R.H.D., MacFarlane, J.J. 2005 *ApJ* 628, 986
- Kraus, S., Weigelt, G., Balega, Y.Y. et al. 2009 *A&A* 497, 195
- Leto, P., Trigilio, C., Buemi, C.S., Umana, G., Leone, F. 2006 *A&A* 458, 831
- Leto, P., Trigilio, C., Oskinova, L. et al. 2017 *MNRAS* 457, 2820
- Linsky, J.L., Drake, S.A., Bastian, T. S. 1992 *ApJ* 393, 341
- Lucy, L.B. 1982, *ApJ*, 255, 286
- Lucy, L.B., & White, R.L. 1980 *ApJ* 241, 300
- Maier, G. et al. (CTA Consortium) 2017, in *Proc. 35th ICRC (Busan, Korea)*, PoS(ICRC2017), 846
- Marchili, N., Piano, G., Cardillo, M., et al. 2018 *A&A*, 615, A82
- Moskalenko, I. V., Porter, T. A., & Digel, S. W. 2006 *ApJ* 652, L65
- Orlando, E., & Strong, A. W. 2007 *Ap&SS* 309, 359
- Orlando, E., & Strong, A. W. 2008 *A&A* 480, 84
- Orlando, E., & Strong, A. W. 2021 *JCAP* 04, 004
- Owocki, S.P., Rybicki, G.B. 1984, *ApJ* 284, 337
- Petit, V., Owocki, S.P., Wade, G.A. et al. 2013 *MNRAS* 429, 398
- Pittard, J. M. & Dougherty, S.M. 2006 *MNRAS* 372, 801
- Pollock, A.M.T. 1987 *ApJ* 320, 283
- Pshirkov, M. S. 2016 *MNRAS* 457, L99
- Reimer, A., Pohl, M., Reimer, O. 2006 *ApJ* 644, 1118

- Revinius, T., Townsend R.H., Kochukhov O. et al. 2013 MNRAS 429, 177
- Shore, S.N. 1987 AJ 94, 731
- Shore, S.N., Brown, D.N. 1990 ApJ 365, 665
- Sierpowska, A., Bednarek, W. 2005 MNRAS 356, 711
- Simón-Díaz, S., Herrero, A., Esteban, C., Najarro, F. 2006 A&A 448, 351
- Stahl, O., Wolf, B., Gang, Th., Gummertsbach, C.A., Kaufer, A., Kovacs, J., Mandel, H., Szeifert, Th. 1993 A&A 274, L29
- Stahl, O., Kaufer, A., Rivinius, T. et al. 1996 A&A 312, 539
- Tam, P.H.T., Huang, R.H.H., Takata, J., Hui, C.Y., Kong, A.K.H., Cheng, K.S. 2011 ApJ 736, L10
- Tavani, M., Sabatini, S., Pian, E. et al. 2009 ApJ 698 L142
- Trigilio, C., Leto, P., Umana, G., Leone, F., Buemi, C.S. 2004 A&A 418, 593
- ud-Doula, A., Owocki, S.P. 2002 ApJ 576, 413
- Usov, V.V., Melrose D.B. 1992 ApJ 395, 575
- Wade, G.A., Fukkerton, A.W., Donati, J.-F., Landstreet, J.D., Petit, P., Strasser, S. 2006 A&A 451, 195
- White, W., & Chen, W. 1992 ApJ 387, 81